Sliding Mode Stabilization and Phase Plane Trajectory Planning for a Cart Pendulum System

9th Semester Project

Nonlinear Systems

Aalborg University
Control & Automation
Fredrik Bajers Vej 7
DK-9220 Aalborg

by
Niels Skov Vestergaard

AALBORG UNIVERSITY
STUDENT REPORT

NTNU

9th Semester

School of Information and Communication Technologies

Control and Automation

Fredrik Bajers Vej 7C

9220 Aalborg

http://www.sict.aau.dk/electronics-and-it

Title:
Sliding Mode Stabilization and Phase Plane Trajectory Planning for a Cart Pendulum System

Theme:
Control Engineering

Project Period:
Autumn 2017
21/08/2017 - 21/12/2017

Participants:
Niels Skov Vestergaard

Supervisor:
Anton Shiriaev
John-Josef Leth

Pages:

Concluded: 15/08/2018

Synopsis

The aim of the project was to develop a sliding mode controller to stabilize a cart pendulum in its unstable equilibrium. Further to investigate a method for trajectory planning for a cart pendulum without friction. To find an interesting trajectory, a task was posed for the system to complete.
The system was modeled using both Newton's method and the energy method. The system was simulated using both simulink and matlab's ode45-solver. To aid in the process and to be able to visually show the results an animation was added to the simulations.
A sliding mode controller stabilizing the pendulum within 0.05 rad was designed and implemented successfully. The posed task for trajectory planning was solved with a minor exception of bringing the pendulum to a compete stop at the end.

Contents

1 | Introduction

The cart pendulum is a common system subjected to different control tasks. It is interesting because it is relatively simple while still being an underactuated, and nonlinear system. This makes it an ideal platform for investigating and comparing control strategies. The system is effectively controlled by a force on the side of the cart and it being underactuated there is no direct control on the pendulum attached to the cart.
This project is two-part. Both parts deals with the cart pendulum system, however, while the first part considers a real system setup with frictions, the second part uses the same parameters but without any friction.
First part contains a description of the supplied system setup and a model derivation first using Newton's method then using the energy method. Finally a sliding mode controller is designed and implemented, both in simulation and in the real system, to stabilize the system in zero.
Second part contains a method for planning trajectories in the phase plane. This enables the possibility of solving tasks where the system is required to move in the nonlinear phase plane. The task solved in this project is seen in Figure 1.1, where the pendulum must follow a planned trajectory to avoid the two obstacles.

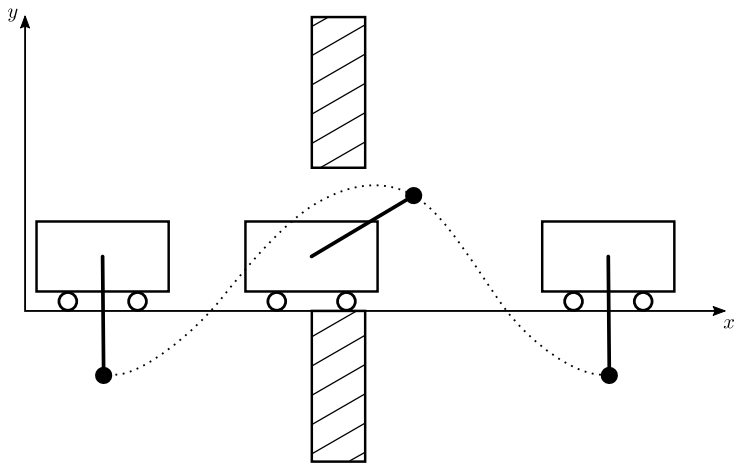

Figure 1.1: The task to be performed in part two. The trajectory here is not realistic, and only shown to illustrate the goal; avoiding the obstacles along the entire trajectory.

As mentioned, friction is removed for the second part. This is both to reduce complexity but also because the system setup is too short for the large movements required to complete the task. The control for this part is therefore run in simulation and an animation is developed to visualize the result.

Part I

System and Stabilization

2 | The System

In this chapter, the system is presented, along with a brief overview of the hardware provided in the setup.

2.1 System Setup

A system is provided by the automation and control department at Aalborg University (AAU). The setup is seen in Figure 2.1, the parameters that can be measured directly are indicated.

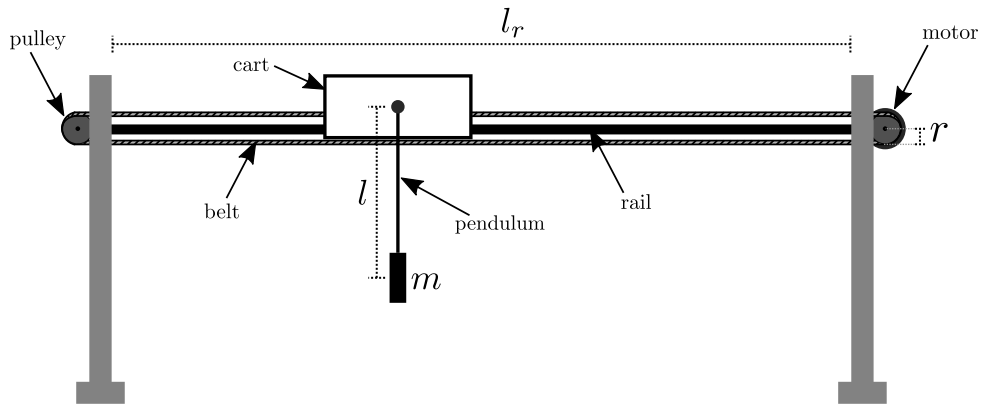

Figure 2.1: The system setup provided by AAU, where m is the mass of the pendulum weight attached at the end of the rod, l is the length from pivot point to center of mass, r is the radius of the pulley and l_r is the effective length of the rail.

The mass of the cart cannot be directly measured as it is preferred not to take the system apart. This parameter is later estimated along with frictions in the system.

2.2 Motors

There are two Maxon 370356 brushed DC motors, see Figure 2.2, used in the setup.[1]

Figure 2.2: The motor used in the setup.[1]

The most interesting characteristic of the maxon motor for the purposes of this report are shown in Table 2.1.

Characteristic	Quantity	Unit
Nominal torque (max. continuous torque)	420×10^{-3}	$\mathrm{N} \cdot \mathrm{m}$
Nominal current (max. continuous current)	4.58	A
Torque constant	93.4×10^{-3}	$\mathrm{N} \cdot \mathrm{m} \cdot \mathrm{A}^{-1}$
Rotor inertia	54.2×10^{-6}	$\mathrm{kg} \cdot \mathrm{m}^2$
Weight	1.1	kg

Table 2.1: Motor characteristics given by [1].

One of the motors is mounted on a pulley driving the belt, see Figure 2.1. The other motor is disabled and acts only as a bearing at the pendulum pivot point.

2.3 Motor Encoders

Each of the two motors are equipped with an HEDS 5540 optical quadrature encoder, see Figure 2.2. The moment of inertia added by the encoder is negligibly small at only $0.6 \times 10^{-6}\,\mathrm{kg} \cdot \mathrm{m}^2$ and is not mentioned further in this report.[2]

Figure 2.3: The encoders used in in this project. [2]

2.4 Motor Controller

Two Maxon ADS 50/10 motor controllers, see Figure 2.4, are mounted on the cart pendulum setup. One on the side to control the driving motor and the other, not used in this project, mounted on the cart. The datasheet states that the motor controller weights 0.38 kg, but again, since the remaining mass of the cart is unknown and can not be measured, the cart mass must be estimated.[3]

Figure 2.4: The Maxon motor controller used in the setup.[3]

The motor controller can be configured in four different modes, [3]

- Speed control using tacho signals
- Speed control using encoder signals
- IxR compensated speed control
- Torque or current control

The first three modes are forms of speed control while the last is current control relating directly to torque and thereby also force on the belt. The chosen mode for this project is therefore current control. The conversion from armature current to motor torque is by use of the torque constant given in Table 2.1. To set the armature current the motor controller requires a $\pm 10\,\mathrm{V}$ input signal [3]. This input is provided through a shield from the microcontroller, so the conversion to armature current is handled in the following.

2.5 Micro Controller

The control design is implemented on a Teensy 3.6 microcontroller, see Figure 2.5, provided in the setup. The armature current reference is provided through one of the microcontroller's two 12 bit DAC's (Digitl-to-Analog Converter) placed on an external pin of the microcontroller. The Teensy 3.6 runs on $3.3\,\mathrm{V}$ provided by an onboard regulator from $5\,\mathrm{V}$ USB supply, and so the analog output is in the range of $0-3.3\,\mathrm{V}$ with a 12 bit resolution.[4]
The motor encoders are decoded on the shield, see next section, and read through an 8 bit parallel data bus by the microcontroller.

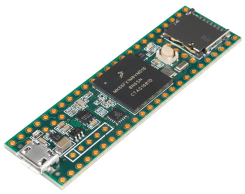

Figure 2.5: The teensy 3.6 used as main control unit in the setup. [5]

The Teensy 3.6 uses a bootloader which allows programming through USB using the Teensyduino add-on for the Arduino IDE.[5]

2.6 Shield

A shield located by the microcontroller handles conversion/interfacing between the microcontroller and the setup. The motor encoders are decoded using Avago HCTL-2021-PLC decoders, mounted on the shield, which outputs 2000 ticks pr. revolution.[6] This results in a resolution of $2\pi/2000 = \pi \times 10^{-3}\,\mathrm{rad/tic}$, for the pendulum angle, θ, and

$2\pi r/2000 = 2\pi \cdot 0.028/2000 \approx 0.088 \times 10^{-3}\,\mathrm{m/tic}$ for the position along x. The armature current reference is provided from the microcontroller which as mentioned outputs $0{-}3.3\,\mathrm{V}$ while the motor controller requires a $\pm 10\,\mathrm{V}$ input. This is handled by an amplification on the shield converting the $0{-}3.3\,\mathrm{V}$ to the required $\pm 10\,\mathrm{V}$. A previous project group has tested the relation between armature current and different 12 bit values from the micro controller. The test was conducted using a current clamp and an oscilloscope to measure the armature current in the motor. By linear regression they arrived at the following relation,

$$\mathrm{bit}_{\mathrm{DAC}} = 105.78 \cdot i_a + 1970 \quad . \tag{2.1}$$

An other way of measuring the current is from an output directly on the motor controller. It is found that this output is slightly different than the current measured directly over the motor using a current clamp. It is difficult to know if the torque constant supplied by the company is matched using one or the other way of measuring. So a test is conducted to verify Equation 2.1, in which the steady state hold force is measured directly on the cart using a luggage scale as an alternative Newton-meter. The results of the force test are seen in Figure 2.6 and 2.7.

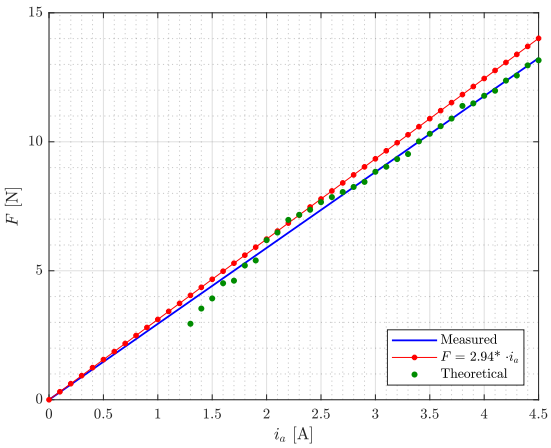

Figure 2.6: Result of force test compared to theoretical result with current model.

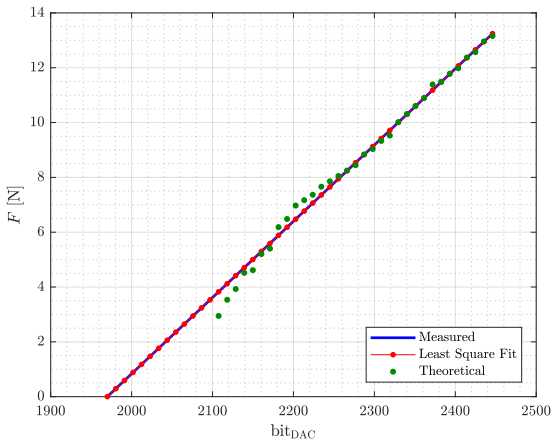

Figure 2.7: Showing how the corrected model for i_a now fits exactly the results of the force test.

The measurements should be more correct at higher forces since friction then causes less disturbance in the measurements. However, no measurements are excluded in the regression as it is noted that the regression line fits the upper part of the data very well. Measurements lower than $F = 2.95$ were considered unreliable due to friction and therefore not included in the data-set. In Figure 2.6 the armature current is scaled using Equation 2.1 and the theoretical line is calculated using that $F = \frac{1}{r} k_\tau i_a$. As the theoretical line does not coincide exactly with the least square regression, Equation 2.1 is tweaked so that,

$$\mathrm{bit}_{\mathrm{DAC}} = 111.9 \cdot i_a + 1970 \quad , \tag{2.2}$$

which leads to the result seen in Figure 2.7, where the theoretical line now coincide with the least square regression of the measurement data.

3 | Modelling

A dynamical model of the system is developed, first by Newton's method and then by the energy method. The model is simulated and the nonlinear nature of the system is investigated.
The model is based on the conventions presented in the mechanical diagram in Figure 3.2 while excessive coordinates are defined in Figure 3.1. The cart is constrained to the horizontal rail s.t. $y_c = 0$, that is, the cart only ever moves along the x-axis.

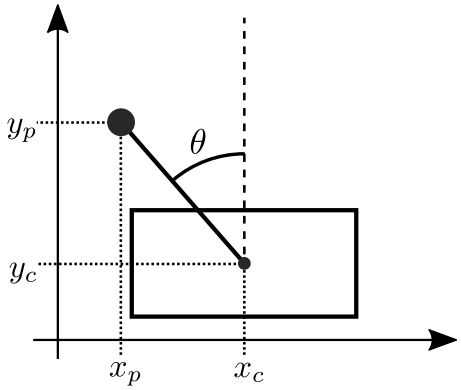

Figure 3.1: The cart pendulum system with excessive coordinates, where (x_c, y_c) is the position of pendulum pivot point on the cart and (x_p, y_p) is the position of the pendulum point mass.

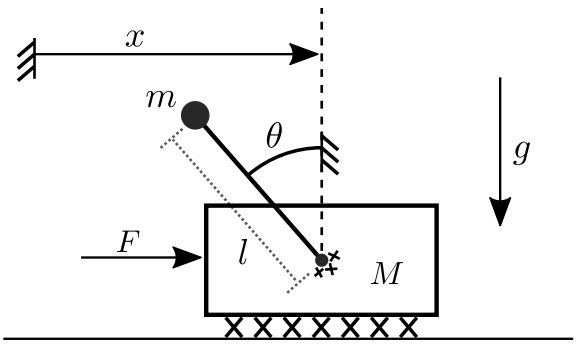

Figure 3.2: Mechanical drawing of the cart pendulum system with x and θ as generalized coordinates, where x is the center position of the cart, θ is the angle of the pendulum, m is the point mass of the pendulum, M is the mass of the cart, g is the gravitational acceleration and F is the force of actuation.

It is assumed that the pendulum rod is rigid and massless. This is deemed sensible, as the pendulum mass is much heavier than the hollow aluminum rod. The added inertia of the motor's rotor is also negligibly small, only $54.2 \times 10^{-6}\,\mathrm{kg \cdot m^2}$, see *Motors* section 2.2, compared to $ml = 0.201 \cdot 0.3348 = 67.3 \times 10^{-3}\,\mathrm{kg \cdot m^2}$ contributed by the pendulum mass. The pendulum mass is modeled as a point mass placed at its geometrical center. This is why the length, l, is measured from the pivot point to the center of the pendulum mass. The mass of the cart includes the weight of the belt and the wires hanging from the cart to the controller and supply. The influence of the wires will vary depending on the position of the cart, but this is treated as an unmodeled disturbance.
In the following two modeling approaches, fictions is represented as two unknown functions of generalized velocities, $\dot{x}$ and $\dot{\theta}$, denoted $B_c(\dot{x})$ for the cart and $B_p(\dot{\theta})$ for the pendulum. These functions are then modeled in section 3.3.

3.1 Newton's Method

Using excessive coordinates, the freebody diagrams are shown in Figure 3.3 and 3.4

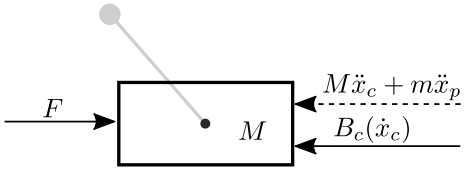

Figure 3.3: Freebody diagram of cart.

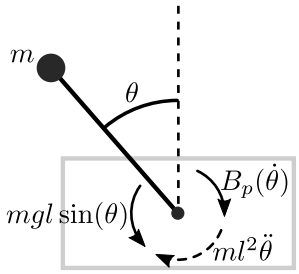

Figure 3.4: Freebodey diagram of pendulum.

Usng Newton's second law for the cart along x_c, see freebody diagram in Figure 3.3,

$$M\ddot{x}_c + m\ddot{x}_p = F - B_c(\dot{x}_c) \quad . \tag{3.1}$$

Applying Newton's second law for rotational motion. Freebody diagram in Figure 3.4

$$ml^2\ddot{\theta} = mgl\sin\theta - B_p(\dot{\theta}) \quad . \tag{3.2}$$

Relation of D'alembert forces for the pendulum decomposed as tangential forces,

$$-m\ddot{x}_p\cos\theta - m\ddot{y}_p\sin\theta = ml\ddot{\theta} \quad . \tag{3.3}$$

To combine Equation 3.3 and 3.2, Equation 3.3 is written as torques,

$$-ml\ddot{x}_p\cos\theta - ml\ddot{y}_p\sin\theta = ml^2\ddot{\theta} \quad , \tag{3.4}$$

Equation 3.3 and 3.2 are combined,

$$-ml\ddot{x}_p\cos\theta - ml\ddot{y}_p\sin\theta = mgl\sin\theta - B_p(\dot{\theta}) \quad . \tag{3.5}$$

The system dynamics is then represented using excessive coordinates by the following set of equations:

$$\begin{cases} -ml\ddot{x}_p\cos\theta - ml\ddot{y}_p\sin\theta = mgl\sin\theta - B_p(\dot{\theta}) \\ M\ddot{x}_c + m\ddot{x}_p = F - B_c(\dot{x}_c) \quad . \end{cases} \quad [\cdot] \tag{3.6}$$

Writing the excessive coordinates, Figure 3.1, in therms of the generalized coordinates, Figure 3.2,

$$\begin{cases} x_c &= x \\ y_c &= 0 \end{cases} \qquad \begin{cases} x_p = x - l\sin\theta \\ y_p = l\cos\theta \end{cases} \quad . \tag{3.7}$$

Finding the derivatives for the transformation,

$$\begin{cases} \dot{x}_p &= \dot{x} - l\cos\theta\dot{\theta} \\ \dot{y}_p &= -l\sin\theta\dot{\theta} \end{cases} \quad \begin{cases} \ddot{x}_p = \ddot{x} + l\sin\theta\dot{\theta}^2 - l\cos\theta\ddot{\theta} \\ \ddot{y}_p = -l\cos\theta\dot{\theta}^2 - l\sin\theta\ddot{\theta} \end{cases} \quad . \tag{3.8}$$

Rewriting Equation 3.6 in generalized coordinates using the coordinate transformation from Equation 3.7 and 3.8 yields,

$$\begin{cases} -ml(\ddot{x} + l\sin\theta\dot{\theta}^2 - l\cos\theta\ddot{\theta})\cos\theta - ml(-l\cos\theta\dot{\theta}^2 - l\sin\theta\ddot{\theta})\sin\theta = mgl\sin\theta - B_p(\dot{\theta}) \\ M\ddot{x} + m(\ddot{x} + l\sin\theta\dot{\theta}^2 - l\cos\theta\ddot{\theta}) = F - B_c(\dot{x}) \quad . \end{cases}$$

$$\begin{cases} ml^2\ddot{\theta} - ml\cos\theta\ddot{x} - mgl\sin\theta &= -B_p(\dot{\theta}) \\ (M+m)\ddot{x} + ml\sin\theta\dot{\theta}^2 - ml\cos\theta\ddot{\theta} &= F - B_c(\dot{x}) \quad , \end{cases} \quad [\cdot] \tag{3.9}$$

which is the final dynamic equations for the cart pendulum system.

3.2 Energy Method

The energy method is applied to find the dynamic equations starting by using excessive coordinates. The potential and kinetic energy for the pendulum is,

$$U_p = mgh \quad [\cdot] \tag{3.10}$$
$$T_p = \tfrac{1}{2}m\dot{x}_p^2 + \tfrac{1}{2}m\dot{y}_p^2 \quad , \quad [\cdot] \tag{3.11}$$

Where:

U_p	is the potential energy of the pendulum	$[\cdot]$
T_p	is the kinetic energy of the pendulum	$[\cdot]$
h	is the height of the pendulum point mass	[m]

where the height, h, is given in relation to the pendulum at rest at $\theta = \pm\pi n$ by,

$$h = l(1 + \cos\theta) \quad . \quad [\cdot] \tag{3.12}$$

The potential and kinetic energy in excessive coordinates for the cart is,

$$U_c = 0 \quad [\cdot] \tag{3.13}$$
$$T_c = \tfrac{1}{2}M\dot{x}_c^2 \quad . \quad [\cdot] \tag{3.14}$$

Where:

U_c	is the potential energy of the cart	$[\cdot]$

T_c is the kinetic energy of the cart $[\cdot]$

There is no potential energy for the cart as it is constrained at $y_c = 0$.
The combined energies for the system in excessive coordinates is then,

$$U = mgl(1 + \cos\theta) + 0 \quad [\cdot] \quad (3.15)$$
$$T = \tfrac{1}{2}m\dot{x}_p^2 + \tfrac{1}{2}m\dot{y}_p^2 + \tfrac{1}{2}M\dot{x}_c^2 \quad , \quad [\cdot] \quad (3.16)$$

Using the coordinate transformation from Equation 3.7 and 3.8 to obtain the energies of the system in generalized coordinates,

$$\begin{cases} U &= mgl(1 + \cos\theta) + 0 \\ T &= \tfrac{1}{2}m(\dot{x} - l\cos\theta\dot{\theta})^2 + \tfrac{1}{2}m(-l\sin\theta\dot{\theta})^2 + \tfrac{1}{2}M\dot{x}^2 \end{cases}$$

$$\begin{cases} U &= mgl(1 + \cos\theta) \\ T &= \tfrac{1}{2}(M+m)\dot{x}^2 - m\dot{x}l\cos\theta\dot{\theta} + \tfrac{1}{2}ml^2\dot{\theta}^2 \quad , \end{cases} \quad [\cdot] \quad (3.17)$$

By Equation 3.17 the Lagrangian becomes,

$$\mathcal{L} = T - U$$
$$\mathcal{L} = \tfrac{1}{2}(M+m)\dot{x}^2 - m\dot{x}l\cos\theta\dot{\theta} + \tfrac{1}{2}ml^2\dot{\theta}^2 - mgl(1 + \cos\theta) \quad . \quad [\mathrm{N}\cdot\mathrm{m}] \quad (3.18)$$

Where:

$\mathcal{L}$ is the Lagrangian $[\mathrm{N}\cdot\mathrm{m}]$

From the energy method we find the dynamic equations by,

$$\frac{\partial\mathcal{L}}{\partial\mathbf{q}} - \frac{d}{dt}\frac{\partial\mathcal{L}}{\partial\dot{\mathbf{q}}} = 0 \quad . \quad (3.19)$$

Where:

$\mathbf{q}$ is the generalized coordinates, $[\ \theta \quad x\ ]^T$

$\dot{\mathbf{q}}$ is the generalized velocities, $[\ \dot{\theta} \quad \dot{x}\ ]^T$

In order to include external forces d'Alambert principle,

$$\frac{d}{dt}\frac{\partial\mathcal{L}}{\partial\dot{\mathbf{q}}} - \frac{\partial\mathcal{L}}{\partial\mathbf{q}} = \mathbf{Q} \quad . \quad (3.20)$$

Where:

$\mathbf{Q}$ is the external forces, $[\ -B_p(\dot{\theta}) \quad F - B_c(\dot{x})\ ]^T$

For yields the final two dynamic equations, one for each of the generalized coordinates,

$$\begin{cases} \frac{d}{dt}\frac{\partial \mathcal{L}}{\partial \dot{\theta}} - \frac{\partial \mathcal{L}}{\partial \theta} & = m\dot{x}l\sin\theta\dot{\theta} - ml\cos\theta\ddot{x} + ml^2\ddot{\theta} - m\dot{x}l\sin\theta\dot{\theta} - mgl\sin\theta \\ \frac{d}{dt}\frac{\partial \mathcal{L}}{\partial \dot{x}} - \frac{\partial \mathcal{L}}{\partial x} & = (M+m)\ddot{x} + ml\sin\theta\dot{\theta}^2 - ml\cos\theta\ddot{\theta} - 0 \end{cases}$$

$$\begin{cases} ml^2\ddot{\theta} - ml\cos\theta\ddot{x} - mgl\sin\theta = -B_p(\dot{\theta}) \\ (M+m)\ddot{x} + ml\sin\theta\dot{\theta}^2 - ml\cos\theta\ddot{\theta} = F - B_c(\dot{x}) \quad , \end{cases} \qquad [\cdot] \quad (3.21)$$

which is the same result as achieved by Newton's method, as seen by comparing Equation 3.9 and 3.21.

3.3 Friction and Motor Model

In the previous, the friction is represented as functions of velocities, $B_c(\dot{x})$ and $B_p(\dot{\theta})$. The frictions are assumed to consist solely of Coulomb and viscous friction. This is a fairly simplified friction model and while it might be advantageous to include further friction dynamics, such as stiction and Stribeck friction, it is considered to be out of scope in this project.

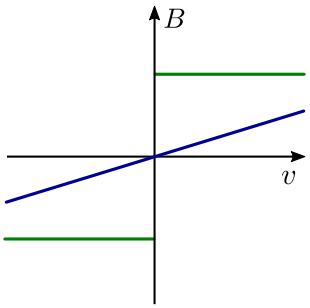

Figure 3.5: coulombViscous1

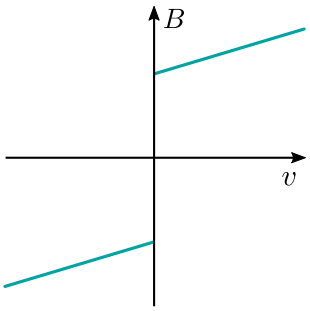

Figure 3.6: coulombViscous2

The Coulomb and viscous friction as sketched in Figure 3.5 and 3.6 are described by the following relations for the pendulum and cart respectively,

$$B_p(\dot{\theta}) = b_{p,v}\dot{\theta} + \text{sgn}(\dot{\theta})b_{p,c} \qquad [\text{N}] \quad (3.22)$$

$$B_c(\dot{x}) = b_{c,v}\dot{x} + \text{sgn}(\dot{x})b_{c,c} \quad . \qquad [\text{N}] \quad (3.23)$$

Where:

$b_{p,v}$	is the pendulum viscous friction	$[\text{N}\cdot\text{m}\cdot\text{s}]$
$b_{p,c}$	is the pendulum coulomb friction	$[\text{N}\cdot\text{m}]$
$b_{c,v}$	is the cart viscous friction	$[\text{N}\cdot\text{m}^{-1}\cdot\text{s}]$
$b_{c,c}$	is the cart coulomb friction	$[\text{N}]$

The sign-function used in Equation 3.23 is undesired, as it introduces a discontinuity at zero velocity. A commonly used continuous approximation of the Coulomb friction is achieved using a tanh-function with a constant, $\mathrm{k_{tanh}}$, to adjust the curve's steepness around zero.

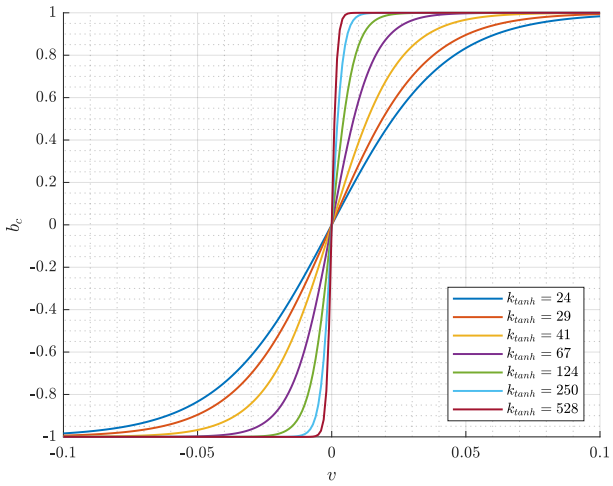

Figure 3.7: tanhApprox

Figure 3.7 shows the tanh approximation with different values of $\mathrm{k_{tanh}}$. The friction parameters were estimated by a previous group who chose $\mathrm{k_{tanh}} = 250$, so it makes sense to choose the same. Further, by comparing the curves in Figure 3.7 the choice of $\mathrm{k_{tanh}}$ seems a reasonable compromise between size of constant and steepness of the curve. The final friction model is then given by,

$$B_p(\dot{\theta}) = b_{p,v}\dot{\theta} + \tanh(\mathrm{k_{tanh}}\dot{\theta})b_{p,c} \quad [\mathrm{N}] \quad (3.24)$$

$$B_c(\dot{x}) = b_{c,v}\dot{x} + \tanh(\mathrm{k_{tanh}}\dot{x})b_{c,c} \quad . \quad [\mathrm{N}] \quad (3.25)$$

The input force so far is represented by F, which is directly applied in the positive x direction on the cart. As seen in the beginning of this chapter in Figure 2.1, this force is applied by a motor mounted with a belt on pulleys. Because the motor control unit is set up in current control mode the electrical motor dynamics are already accounted for. The controllable input is therefore the motor current, i_a. The torque, τ_m of the motor is modeled as directly proportional to the motor current by a torque constant, k_τ, as stated in *Motors* section 2.2,

$$\tau_m = k_\tau i_a \quad [\mathrm{N \cdot m}] \quad (3.26)$$

To translate this torque to the belt it is divided by the radius, r, of the pulley,

$$F = \tfrac{1}{r} k_\tau i_a \quad [\mathrm{N}] \quad (3.27)$$

3.4 Parameters

As mentioned, some parameters could not be measured directly. These parameter were estimated by a previous group[7]. A table of the values they estimated along with directly measurable values are stated in Table 3.1.

Parameter	**Notation**	**Quantity**	**Unit**
Pendulum Mass	m		kg
Cart Mass *	M		kg
Rod Length	l		m
Pulley Radius	r		m
Cart Coulomb Friction *	$b_{c,c}$		N
Cart Viscous Friction *	$b_{c,v}$		$\mathrm{N{\cdot}m^{-1}{\cdot}s}$
Pendulum Coulomb Friction *	$b_{p,c}$		N·m
Pendulum Viscous Friction *	$b_{p,v}$		N·m·s

Table 3.1: '*' indicates that the parameter is estimated.

Though the inertia of the rotor is stated in the datasheet of the motor, see *Motors* section 2.2, the added inertia and mass of from the pulley and belt is unknown. Further, both viscous and Coulomb friction on the cart are assumed purely translational. Similarly, though the weights of motor and motor controller mounted on the cart are known, the collective weight of the cart is unknown. For these reasons, the cart weight, viscous and Coulomb friction were estimated by the previous group such that they include friction and inertia added by the motor, belt and pulleys.[7]

4 | Nonlinear Control

The control objective is to stabilize the pendulum at $\theta = 0$. To achieve this objective a sliding mode controller is designed for the cart pendulum system. To do so the system is transformed into a *regular form* presented in this chapter along with the sliding mode design.

4.1 System Transformation

To develop a sliding mode controller, the system is first transformed into a *regular form*,

$$\dot{\boldsymbol{\eta}} = f_a(\boldsymbol{\eta}, \boldsymbol{\xi}) \tag{4.1}$$

$$\dot{\boldsymbol{\xi}} = f_b(\boldsymbol{\eta}, \boldsymbol{\xi}) + g_b(\boldsymbol{\eta}, \boldsymbol{\xi})F \quad . \tag{4.2}$$

The system is first presented on nonlinear state space form, from Equation 3.21,

$$\begin{bmatrix} ml^2 & -ml\cos\theta \\ -ml\cos\theta & M+m \end{bmatrix} \begin{bmatrix} \ddot{\theta} \\ \ddot{x} \end{bmatrix} + \begin{bmatrix} -mgl\sin\theta \\ ml\sin\theta\dot{\theta}^2 \end{bmatrix} = \begin{bmatrix} -B_p(\dot{\theta}) \\ F - B_c(\dot{x}) \end{bmatrix} \tag{4.3}$$

By rearranging Equation 4.3,

$$\begin{bmatrix} ml^2 & -ml\cos\theta \\ -ml\cos\theta & M+m \end{bmatrix} \begin{bmatrix} \ddot{\theta} \\ \ddot{x} \end{bmatrix} + \begin{bmatrix} 0 \\ ml\sin\theta\dot{\theta}^2 \end{bmatrix} + \begin{bmatrix} B_p(\dot{\theta}) \\ B_c(\dot{x}) \end{bmatrix} + \begin{bmatrix} -mgl\sin\theta \\ 0 \end{bmatrix} = \begin{bmatrix} 0 \\ F \end{bmatrix} \quad , \tag{4.4}$$

the achieved form is that of the general dynamic equations for an m-link robot, [8, 9]

$$\mathbf{M}(\mathbf{q})\ddot{\mathbf{q}} + \mathbf{C}(\mathbf{q}, \dot{\mathbf{q}}) + \mathbf{B}(\dot{\mathbf{q}}) + \mathbf{G}(\mathbf{q}) = \mathbf{F} \quad . \tag{4.5}$$

Where:

$\mathbf{M}(\mathbf{q})\ddot{\mathbf{q}}$	is the inertia matrix
$\mathbf{C}(\mathbf{q}, \dot{\mathbf{q}})$	is the Coriolis and centrifugal effects
$\mathbf{B}(\dot{\mathbf{q}})$	is the friction
$\mathbf{G}(\mathbf{q})$	is the force due to gravity
$\mathbf{F}$	is the input force

Isolating the accelerations,

$$\ddot{\mathbf{q}} = \mathbf{M}^{-1}(\mathbf{q})\left(\mathbf{F} - \mathbf{C}(\mathbf{q}, \dot{\mathbf{q}}) - \mathbf{B}(\dot{\mathbf{q}}) - \mathbf{G}(\mathbf{q})\right) \quad , \tag{4.6}$$

and choosing the state vector to be $[\ x_1\ x_2\ x_3\ x_4\ ]^T = [\ \theta\ x\ \dot{\theta}\ \dot{x}\ ]^T$, the nonlinear state space representation is then,

$$\begin{bmatrix} \dot{x_1} \\ \dot{x_2} \\ \dot{x_3} \\ \dot{x_4} \end{bmatrix} = \begin{bmatrix} x_3 \\ x_4 \\ \mathbf{M}^{-1}(x_1)\left(-\mathbf{C}(x_1, x_3) - \mathbf{B}(x_3, x_4) - \mathbf{G}(x_1)\right) \end{bmatrix} + \begin{bmatrix} 0 \\ 0 \\ \mathbf{M}^{-1}(x_1) \begin{bmatrix} 0 \\ F \end{bmatrix} \end{bmatrix} \quad , \tag{4.7}$$

where,

$$\mathbf{M}^{-1} = \frac{1}{\det(\mathbf{M})}\text{adj}(\mathbf{M}) = \begin{bmatrix} \frac{(M+m)}{l^2 m(M+m-m\cos^2 x_1)} & \frac{\cos x_1}{l(M+m-m\cos^2 x_1)} \\ \frac{\cos x_1}{l(M+m-m\cos^2 x_1)} & \frac{1}{M+m-m\cos^2 x_1} \end{bmatrix} \quad . \tag{4.8}$$

Introducing following notation,

$$\begin{bmatrix} \dot{x_1} \\ \dot{x_2} \\ \dot{x_3} \\ \dot{x_4} \end{bmatrix} = \underbrace{\begin{bmatrix} x_3 \\ x_4 \\ f_1(\mathbf{x}) \\ f_2(\mathbf{x}) \end{bmatrix}}_{f(\mathbf{x})} + \underbrace{\begin{bmatrix} 0 \\ 0 \\ \frac{\cos x_1}{l(M+m-m\cos^2 x_1)} \\ \frac{1}{M+m-m\cos^2 x_1} \end{bmatrix}}_{g(\mathbf{x})} F \quad . \tag{4.9}$$

where,

$$f_1(\mathbf{x}) = \frac{(M+m)(-B_p(x_3) + mgl\sin x_1)}{l^2 m(M+m-m\cos^2 x_1)} - \frac{\cos x_1(ml\sin x_1 x_3^2 + B_c(x_4))}{l(M+m-m\cos^2 x_1)} \tag{4.10}$$

$$f_2(\mathbf{x}) = \frac{\cos x_1(-B_p(x_3) + mgl\sin x_1)}{l(M+m-m\cos^2 x_1)} - \frac{ml\sin x_1 x_3^2 + B_c(x_4)}{M+m-m\cos^2 x_1} \quad , \tag{4.11}$$

to reduce notation in the derivation of the transformation into *regular form*.

Choosing the pendulum angle as the output s.t. $y = h(\mathbf{x}) = x_1$, the relative degree is found by,

$$\dot{y} = \dot{x_1} = x_3 \tag{4.12}$$

$$\ddot{y} = \dot{x_3} = f_1(\mathbf{x}) + \frac{\cos x_1}{l(M+m-m\cos^2 x_1)} F \quad , \tag{4.13}$$

where the output is found in the second derivative of the output, resulting in relative degree of two, $\rho = 2$, which gives rise to the following transform ,

$$T(\mathbf{x}) = \begin{bmatrix} \boldsymbol{\phi}(\mathbf{x}) \\ \hdashline \boldsymbol{\psi}(\mathbf{x}) \end{bmatrix} = \begin{bmatrix} \phi_1(\mathbf{x}) \\ \phi_2(\mathbf{x}) \\ \hdashline h(\mathbf{x}) \\ L_f h(\mathbf{x}) \end{bmatrix} = \begin{bmatrix} \phi_1(\mathbf{x}) \\ \phi_2(\mathbf{x}) \\ \hdashline x_1 \\ x_3 \end{bmatrix} \quad , \tag{4.14}$$

where $L_f h(\mathbf{x})$ is the *Lie derivative* of $h(\mathbf{x})$ along $f(\mathbf{x})$. The functions $\phi_i(\mathbf{x})$ are chosen such that they satisfy,

$$\frac{\partial \phi_i}{\partial \mathbf{x}} g(\mathbf{x}) = 0 \ , \quad \text{for } 1 \leq i \leq 2 \quad , \tag{4.15}$$

which ensures that the input cancels in $\frac{d\boldsymbol{\phi}}{dt} = \frac{\partial \boldsymbol{\phi}}{\partial \mathbf{x}}[f(\mathbf{x}) + g(\mathbf{x})F]$,

Both $\phi_1(\mathbf{x}) = x_1$ and $\phi_1(\mathbf{x}) = x_2$ would satisfy Equation 4.15, however $\phi_1(\mathbf{x}) = x_1$ would result in a rank defisit in $T(\mathbf{x})$, so $\phi_1(\mathbf{x}) = x_2$ is chosen. For $\phi_2(\mathbf{x})$, it follows from Equation 4.15 that,

$$\frac{\partial \phi_2}{\partial x_3} \cdot \frac{\cos x_1}{l(M + m - m\cos^2 x_1)} + \frac{\partial \phi_2}{\partial x_4} \cdot \frac{1}{M + m - m\cos^2 x_1} = 0 \tag{4.16}$$

$$\frac{\partial \phi_2}{\partial x_3} \cdot \frac{\cos x_1}{l(M + m - m\cos^2 x_1)} + \frac{\partial \phi_2}{\partial x_4} \cdot \frac{l}{l(M + m - m\cos^2 x_1)} = 0 \quad . \tag{4.17}$$

It is attempted to cancel the two therms in Equation 4.17 by choosing,

$$\frac{\partial \phi_2}{\partial x_3} = l \quad , \qquad \frac{\partial \phi_2}{\partial x_4} = -\cos x_1 \tag{4.18}$$

$$\phi_2 = l \int dx_3 - \cos x_1 \int dx_4 \tag{4.19}$$

$$\phi_2 = l x_3 - \cos x_1 x_4 + \mathrm{C}_1 \quad , \tag{4.20}$$

where C_1 is an integration constant. It is also required that $\phi(0) = 0$, so $\mathrm{C}_1 = 0$, resulting in the final transformation,

$$T(\mathbf{x}) = \begin{bmatrix} x_2 \\ l x_3 - \cos x_1 x_4 \\ x_1 \\ x_3 \end{bmatrix} \quad . \tag{4.21}$$

Locating the input in the derivative of the transform,

$$\frac{d}{dt} T(\mathbf{x}) = \begin{bmatrix} \dot{x}_2 \\ l\dot{x}_3 + \sin x_1 x_4 \dot{x}_1 - \cos x_1 \dot{x}_4 \\ \dot{x}_1 \\ \dot{x}_3 \end{bmatrix} \quad . \tag{4.22}$$

Both $\dot{x}_3$ and $\dot{x}_3$ contains the input, so the second element, $\frac{\partial}{\partial \mathbf{x}} T_2(\mathbf{x})$, is further evaluated by substitution of the state derivatives from Equation 4.9,

$$\frac{d}{dt} T_2(\mathbf{x}) = l(f_1(\mathbf{x}) + \tfrac{\cos x_1}{l(M+m-m\cos^2 x_1)} F) + \sin x_1 x_4 x_3 - \cos x_1 (f_2(\mathbf{x}) + \tfrac{1}{M+m-m\cos^2 x_1} F) \tag{4.23}$$

$$\frac{d}{dt} T_2(\mathbf{x}) = \sin x_1 x_4 x_3 + l f_1(\mathbf{x}) - \cos x_1 f_2(\mathbf{x}) \quad , \tag{4.24}$$

showing that the input only appears on the fourth element in the derivative of the transformation. This leads to choosing $[\ \phi_1\ \phi_2\ \psi_1\ \psi_2\ ]^T = [\ \eta_1\ \eta_2\ \eta_3\ \xi\ ]^T$, according to Equation 4.1 and 4.2, as the new variables, with its derivatives,

$$\begin{bmatrix} \dot{\eta}_1 \\ \dot{\eta}_2 \\ \dot{\eta}_3 \\ \dot{\xi} \end{bmatrix} = \overbrace{\underbrace{\begin{bmatrix} x_4 \\ \sin x_1 x_4 x_3 + l f_1(\mathbf{x}) - \cos x_1 f_2(\mathbf{x}) \\ x_3 \\ f_1(\mathbf{x}) \end{bmatrix}}_{f_b}}^{f_a} + \underbrace{\begin{bmatrix} 0 \\ 0 \\ 0 \\ \frac{\cos x_1}{l(M+m-m\cos^2 x_1)} \end{bmatrix}}_{g_b} F \quad , \tag{4.25}$$

which is the system on *regular form*, however, to achieve the full change of variables, s.t.

$$\dot{\boldsymbol{\eta}} = f_a(\boldsymbol{\eta}, \xi) \tag{4.26}$$

$$\dot{\xi} = f_b(\boldsymbol{\eta}, \xi) + g_b(\boldsymbol{\eta}, \xi) F \quad , \tag{4.27}$$

the inverse transform is found,

$$\begin{bmatrix} \eta_1 \\ \eta_2 \\ \eta_3 \\ \xi \end{bmatrix} = \begin{bmatrix} x_2 \\ l x_3 - \cos x_1 x_4 \\ x_1 \\ x_3 \end{bmatrix} \qquad \begin{bmatrix} x_1 \\ x_2 \\ x_3 \\ x_4 \end{bmatrix} = \begin{bmatrix} \eta_3 \\ \eta_1 \\ \xi \\ \frac{l\xi - \eta_2}{\cos \eta_3} \end{bmatrix} \quad , \tag{4.28}$$

to then formulate Equation 4.25 in therms of $[\ \eta_1\ \eta_2\ \eta_3\ \xi\ ]^T$,

$$\begin{bmatrix} \dot{\eta}_1 \\ \dot{\eta}_2 \\ \dot{\eta}_3 \\ \dot{\xi} \end{bmatrix} = \begin{bmatrix} \frac{l\xi - \eta_2}{\cos \eta_3} \\ \frac{\sin \eta_3}{\cos \eta_3}(l\xi - \eta_2)\xi + l f_1(\boldsymbol{\eta}, \xi) - \cos \eta_3 f_2(\boldsymbol{\eta}, \xi) \\ \xi \\ f_1(\boldsymbol{\eta}, \xi) \end{bmatrix} + \begin{bmatrix} 0 \\ 0 \\ 0 \\ \frac{\cos \eta_3}{l(M+m-m\cos^2 \eta_3)} \end{bmatrix} F \quad , \tag{4.29}$$

where,

$$f_1(\boldsymbol{\eta}, \xi) = \frac{(M+m)(mgl \sin \eta_3 - b_{p,v}\xi - \tanh(\mathrm{k}_{\tanh}\xi) b_{p,c})}{l^2 m (M + m - m\cos^2 \eta_3)} \tag{4.30}$$

$$- \frac{\cos \eta_3 (ml \sin \eta_3 \xi^2 + b_{c,v} \frac{l\xi - \eta_2}{\cos \eta_3} + \tanh(\mathrm{k}_{\tanh} \frac{l\xi - \eta_2}{\cos \eta_3}) b_{c,c})}{l(M + m - m\cos^2 \eta_3)} \tag{4.31}$$

$$f_2(\boldsymbol{\eta}, \xi) = \frac{\cos \eta_3 (mgl \sin \eta_3 - b_{p,v}\xi - \tanh(\mathrm{k}_{\tanh}\xi) b_{p,c})}{l(M + m - m\cos^2 \eta_3)} \tag{4.32}$$

$$- \frac{ml \sin \eta_3 \xi^2 + b_{c,v} \frac{l\xi - \eta_2}{\cos \eta_3} + \tanh(\mathrm{k}_{\tanh} \frac{l\xi - \eta_2}{\cos \eta_3}) b_{c,c}}{M + m - m\cos^2 \eta_3} \quad . \tag{4.33}$$

4.2 Sliding Mode

Now, with the system on *regular form*, the sliding mode controller can be designed. The sliding manifold is chosen:

$$s = \xi - \phi(\boldsymbol{\eta}) = 0 \quad , \tag{4.34}$$

where $\phi(\boldsymbol{\eta})$ must be designed. When the system is restricted to move along $s = 0$ then $\xi = \phi(\boldsymbol{\eta})$, which means the reduced-order model,

$$\dot{\boldsymbol{\eta}} = f_a(\boldsymbol{\eta}, \phi(\boldsymbol{\eta})) \quad , \tag{4.35}$$

is asymptotically stable in its origin. To find a stabilizing controller, $\phi(\boldsymbol{\eta})$, for Equation 4.35, the reduced-order system is linearized,

$$A = \frac{\partial \dot{\boldsymbol{\eta}}}{\partial \boldsymbol{\eta}}\bigg|_{\substack{\boldsymbol{\eta}=\mathbf{0} \\ \xi=0 \\ \mathrm{k_{tanh}}=1}} = \begin{bmatrix} 0 & -1 & 0 \\ 0 & \frac{g_{p,c}}{lm} & g \\ 0 & 0 & 0 \end{bmatrix} \quad , \quad B = \frac{\partial \dot{\boldsymbol{\eta}}}{\partial \xi}\bigg|_{\substack{\boldsymbol{\eta}=\mathbf{0} \\ \xi=0 \\ \mathrm{k_{tanh}}=1}} = \begin{bmatrix} l \\ \frac{-b_{p,v}-b_{p,c}}{lm} \\ 1 \end{bmatrix} \quad , \tag{4.36}$$

Using the matlab *place()* command, different pole-placements were attempted, seen in Figure 4.1. The chosen pole placement is $[\ -3 \quad -5 \quad -8\ ]$ resulting in the state feedback gains, $\mathbf{k} = [\ -12.22 \quad 8.05 \quad 20.10\ ]$, of which the result is seen in Figure 4.2, where the linear simulation is achieved using *lsim()* and the nonlinear using *ode45*.

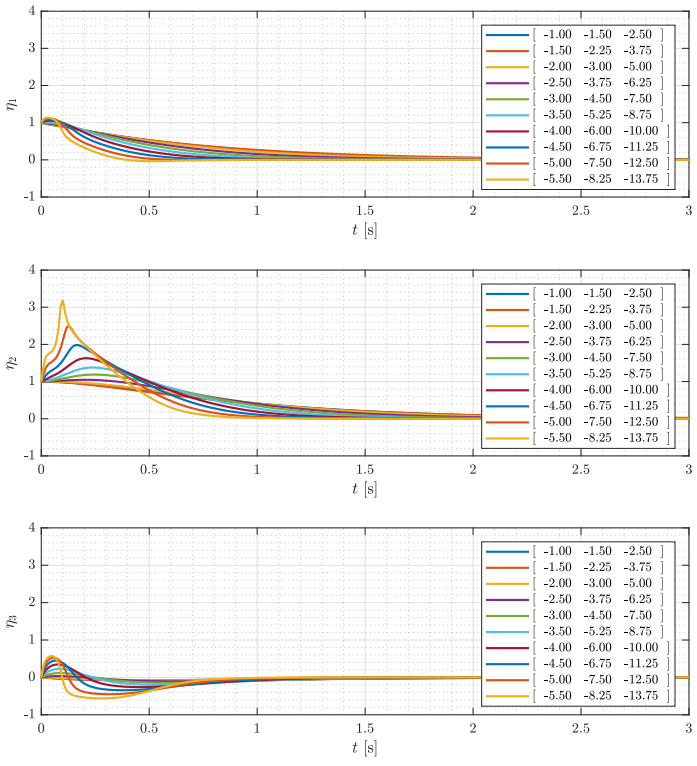

Figure 4.1: reducedOrderControlMany

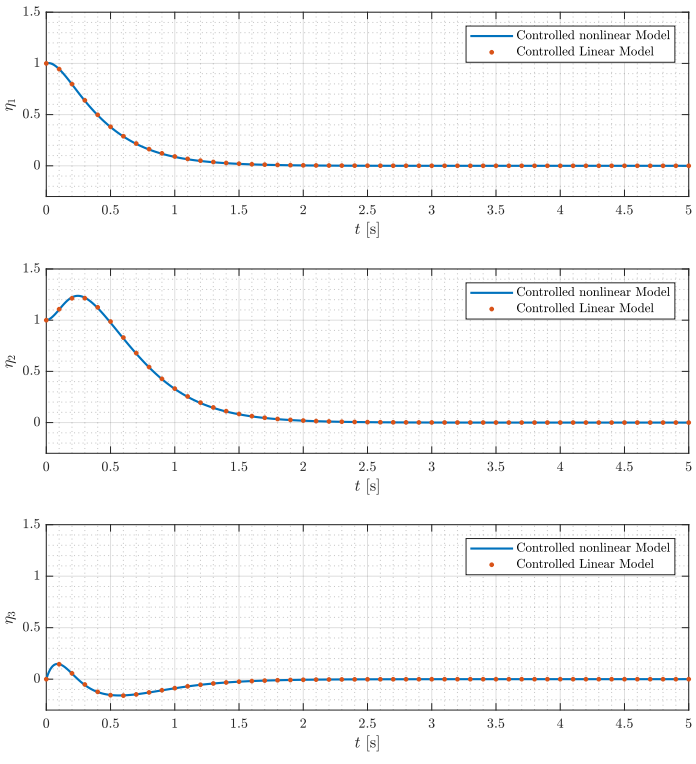

Figure 4.2: reducedOrderControl

With the reduced-order system stabilized by,

$$\phi(\boldsymbol{\eta}) = -\mathbf{k}\boldsymbol{\eta} \quad , \tag{4.37}$$

next step is to design F to bring s to zero.
First a Lyapunov function candidate, $V = \frac{1}{2}s^2$, is chosen and its derivative along the system's trajectories is found,

$$\dot{V} = s\dot{s} \tag{4.38}$$
$$\dot{V} = s(\dot{\xi} + \mathbf{k}\dot{\boldsymbol{\eta}}) \tag{4.39}$$
$$\dot{V} = s(f_b(\boldsymbol{\eta},\xi) + g_b(\boldsymbol{\eta},\xi)F + \mathbf{k}f_a(\boldsymbol{\eta},\xi)) \tag{4.40}$$
$$\dot{V} = (\mathbf{k}f_a(\boldsymbol{\eta},\xi) + f_b(\boldsymbol{\eta},\xi))s + g_b(\boldsymbol{\eta},\xi)sF \tag{4.41}$$
$$\dot{V} = g_b(\boldsymbol{\eta},\xi)s(\mathbf{k}f_a(\boldsymbol{\eta},\xi) + f_b(\boldsymbol{\eta},\xi))g_b^{-1}(\boldsymbol{\eta},\xi) + g_b(\boldsymbol{\eta},\xi)sF \tag{4.42}$$
$$\dot{V} \leq g_b(\boldsymbol{\eta},\xi)|s|\left|\mathbf{k}f_a(\boldsymbol{\eta},\xi)g_b^{-1}(\boldsymbol{\eta},\xi) + f_b(\boldsymbol{\eta},\xi)\right| + g_b(\boldsymbol{\eta},\xi)sF \quad . \tag{4.43}$$

Using that $|s| = \text{sgn}(s)s$ to design F such that the two terms in Equation 4.43 cancels and the stability criterion is fulfilled,

$$\begin{aligned}\dot{V} \leq\ & g_b(\boldsymbol{\eta},\xi)|s|\,|\mathbf{k}f_a(\boldsymbol{\eta},\xi) + f_b(\boldsymbol{\eta},\xi)|\,g_b^{-1}(\boldsymbol{\eta},\xi) \\ & - g_b(\boldsymbol{\eta},\xi)\text{sgn}(s)s\,|\mathbf{k}f_a(\boldsymbol{\eta},\xi) + f_b(\boldsymbol{\eta},\xi)|\,g_b^{-1}(\boldsymbol{\eta},\xi)\end{aligned} \tag{4.44}$$

s.t.

$$F = -\text{sgn}(s)\varrho(\boldsymbol{\eta},\xi)g_b^{-1}(\boldsymbol{\eta},\xi) \quad \text{where,} \quad \varrho(\boldsymbol{\eta},\xi) \geq |\mathbf{k}f_a(\boldsymbol{\eta},\xi) + f_b(\boldsymbol{\eta},\xi)| \quad , \tag{4.45}$$

further, a tuning parameter, β_0, is introduced,

$$F = -\text{sgn}(s)\beta(\boldsymbol{\eta},\xi)g_b^{-1}(\boldsymbol{\eta},\xi) \quad \text{where,} \quad \beta(\boldsymbol{\eta},\xi) = \varrho(\boldsymbol{\eta},\xi) + \beta_0 \quad . \tag{4.46}$$

The sign-function in the control-law, Equation 4.46, introduces a discontinuity around the sliding manifold, which becomes a problem due to delay in a real system, introducing chatter around $s = 0$. To rectify this problem a saturation function is used as a continuous approximation of the sign-function,

$$\text{sat}\left(\tfrac{s}{\varepsilon}\right) = \begin{cases} \frac{s}{\varepsilon}, & \text{if } |\frac{s}{\varepsilon}| \leq 1 \\ \text{sgn}\left(\frac{s}{\varepsilon}\right), & \text{if } |\frac{s}{\varepsilon}| > 1 \end{cases} \quad , \tag{4.47}$$

where $\frac{1}{\varepsilon}$ defines the slope of the saturation function around zero. Finally the control law becomes,

$$F = -\text{sat}(\tfrac{s}{\varepsilon})\beta(\boldsymbol{\eta},\xi)g_b^{-1}(\boldsymbol{\eta},\xi) \quad \text{where,} \quad \beta(\boldsymbol{\eta},\xi) = \varrho(\boldsymbol{\eta},\xi) + \beta_0 \quad . \tag{4.48}$$

The gain design is based on a maximum possible catch angle, $\theta_{\max}$, which is defined from zero angular velocity. The position and velocity along x does not interfere with the value of $\theta_{\max}$, so long as the angular velocity of the pendulum is zero. Note, if the pendulum is

falling away from equilibrium, its non-zero angular velocity will work against the controller and the catch angle will be smaller. However, similarly, if the pendulum is approaching equilibrium, the controller's catch angle will be larger.
While there will be other combinations of θ and $\dot{\theta}$ in the region of interest requiring as much actuation as $(\theta, \dot{\theta}) = (\theta_{\max}, 0)$, these initial values are chosen to be on the edge of the region in the proceeding design.
In Figure 4.3, $\varrho(\boldsymbol{\eta}, \xi)$ and the required peak armature current magnitude, $|i_{a,\text{peak}}|$, are plotted for different initial angles, θinit, to see how large a gain is feasible while staying within the actuation limitation of the motor, $i_{a,\max} = 4.58\,\text{A}$, see *Motors* section 2.2.

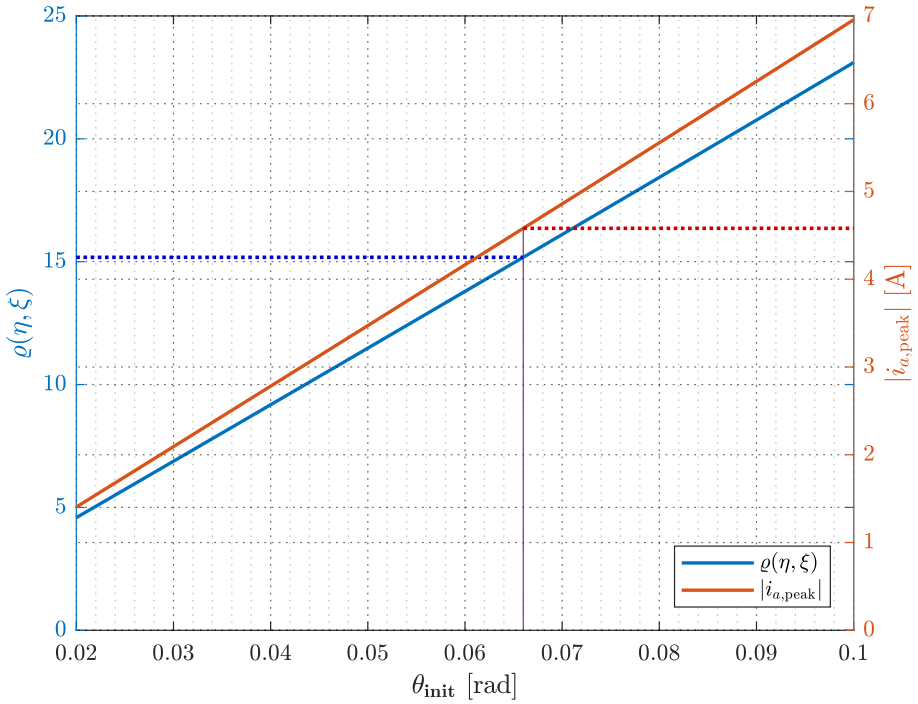

Figure 4.3: $\dot{\theta} = 0$ horizontal line marks $\theta_{\max} = 0.0660$ dictated by the current limitation of the motor, $i_{a,\max} = 4.58\,\text{A}$, and thereby indicating the maximum gain, $\varrho(\boldsymbol{\eta}, \xi) = 15.1776$, with $\beta_0 = 0.1$, allowing some margin for the supposed operational region.

Part II

Phase Plane Trajectory Planning

5 | System and Trajectories

This part is based on [10]. The same cart pendulum system is considered, however to reduce complexity in presenting the concept, the system is considered without friction, so from Equation 3.21 the system is reduced to,

$$\begin{cases} ml^2\ddot{\theta} - ml\cos\theta\ddot{x} - mgl\sin\theta = 0 \\ (M+m)\ddot{x} + ml\sin\theta\dot{\theta}^2 - ml\cos\theta\ddot{\theta} = F \end{cases} \quad . \tag{5.1}$$

[·]

The system is first converted into a *general form* where θ is chosen as the motion generator s.t.,

$$\alpha(\theta)\ddot{\theta} + \beta(\theta)\dot{\theta}^2 + \gamma(\theta) = 0 \quad , \tag{5.2}$$

To achieve this form $\ddot{x}$ is first isolated in the second of the dynamic equations, Equation 3.21,

$$\ddot{x} = \frac{1}{M+m}(F - ml\sin\theta\dot{\theta}^2 + ml\cos\theta\ddot{\theta}) \quad . \tag{5.3}$$

and then substituted for $\ddot{x}$ in the first dynamic equation to obtain,

$$ml^2\ddot{\theta} - ml\cos\theta\left(\frac{1}{M+m}(F - ml\sin\theta\dot{\theta}^2 + ml\cos\theta\ddot{\theta})\right) - mgl\sin\theta = 0 \quad . \tag{5.4}$$

Rearranging yields,

$$\underbrace{\left(ml^2 - \frac{m^2l^2}{M+m}\cos^2\theta\right)}_{\alpha(\theta)}\ddot{\theta} + \underbrace{\left(\frac{m^2l^2}{M+m}\cos\theta\sin\theta\right)}_{\beta(\theta)}\dot{\theta}^2 \underbrace{-mgl\sin\theta - \frac{ml}{M+m}\cos\theta F}_{\gamma(\theta)} = 0 \quad , \tag{5.5}$$

which is the reduced system on the general form from Equation 5.2. The reduced system on nonlinear state space form, where $x_1 = \theta$ and $x_2 = \dot{\theta}$, is given by,

$$\begin{aligned} \dot{x_1} &= x_2 \\ \dot{x_2} &= -\frac{\beta(x_1)}{\alpha(x_1)}x_2^2 - \frac{\gamma(x_1)}{\alpha(x_1)} \end{aligned} \quad , \tag{5.6}$$

which is a convinent representation for creating phase portraits in the $(\theta, \dot{\theta})$-plane.

When planning a trajectory in the $(\theta, \dot{\theta})$-plane, it is assumed that the initial values are known, along with desired final values. If Equation 5.2 is integrated, it is possible to formulate an initial value problem based on the system dynamics. To that end, a change of variable is introduced, $Y = \dot{\theta}^2$, which leads to,

$$\frac{dY}{d\theta} = 2\ddot{\theta} \quad \Rightarrow \quad \ddot{\theta} = \frac{1}{2}\frac{dY}{d\theta} \quad , \tag{5.7}$$

such that, $(\dot{\theta}^2, \ddot{\theta}) = (Y,\ \frac{1}{2}\frac{dY}{d\theta})$. This change of variables is applied to Equation 5.2,

$$\alpha(\theta)\frac{1}{2}\frac{dY}{d\theta} + \beta(\theta)Y + \gamma(\theta) = 0 \quad . \tag{5.8}$$

It is assumed that $\alpha(\theta) > 0$ allowing,

$$\frac{dY}{d\theta} + \frac{2\beta(\theta)}{\alpha(\theta)}Y = -\frac{2\gamma(\theta)}{\alpha(\theta)} \quad . \tag{5.9}$$

Using reduced notation, $P(\theta) = \frac{2\beta(\theta)}{\alpha(\theta)}$ and $Q(\theta) = -\frac{2\gamma(\theta)}{\alpha(\theta)}$, to obtain,

$$\frac{dY}{d\theta} + P(\theta)Y = Q(\theta) \quad , \tag{5.10}$$

selecting $e^{\int P(\theta)d\theta}$ as integration factor,

$$\left(\frac{dY}{d\theta}\right)e^{\int P(\theta)d\theta} + P(\theta)Ye^{\int P(\theta)d\theta} = Q(\theta)e^{\int P(\theta)d\theta} \quad , \tag{5.11}$$

and by use of the product rule,

$$\frac{d}{d\theta}Ye^{\int P(\theta)d\theta} = Q(\theta)e^{\int P(\theta)d\theta} \quad , \tag{5.12}$$

the integral given by,

$$\int \frac{d}{d\theta}Ye^{\int P(\theta)d\theta}d\theta = \int Q(\theta)e^{\int P(\theta)d\theta}d\theta \quad , \tag{5.13}$$

yields the general solution,

$$Y = e^{-\int P(\theta)d\theta}\left(\int Q(\theta)e^{\int P(\theta)d\theta}d\theta + \mathrm{C}_1\right) \quad . \tag{5.14}$$

The integration constant is found by evaluating at time zero, $(\theta(0), \dot{\theta}(0)) = (\theta_0, \dot{\theta}_0)$, thus removing the integrals such that $\mathrm{C}_1 = Y(\theta_0, \dot{\theta}_0) = \dot{\theta}_0^2$. Substituting $P(\theta) = \frac{2\beta(\theta)}{\alpha(\theta)}$, $Q(\theta) = -\frac{2\gamma(\theta)}{\alpha(\theta)}$, $Y = \dot{\theta}^2$ and $\mathrm{C}_1 = \dot{\theta}_0^2$ back into Equation 5.14 yields,

$$\dot{\theta}^2 - \exp\left[-\int \frac{2\beta(\theta)}{\alpha(\theta)}d\theta\right]\left(\dot{\theta}_0^2 - \int \frac{2\gamma(\theta)}{\alpha(\theta)}\exp\left[\int \frac{2\beta(\theta)}{\alpha(\theta)}d\theta\right]d\theta\right) = 0 \quad . \tag{5.15}$$

Finally, by introducing limits,

$$I(\theta, \dot{\theta}, \theta_0, \dot{\theta}_0) = \dot{\theta}^2 - \exp\left[-2\int_{\theta_0}^{\theta}\frac{\beta(\tau)}{\alpha(\tau)}d\tau\right]\left(\dot{\theta}_0^2 - \int_{\theta_0}^{\theta}\exp\left[2\int_{\theta_0}^{s}\frac{\beta(\tau)}{\alpha(\tau)}d\tau\right]\frac{2\gamma(s)}{\alpha(s)}ds\right) \quad , \tag{5.16}$$

where $I(\theta, \dot{\theta}, \theta_0, \dot{\theta}_0) = 0$, the desired integral representation of the system dynamics is achieved. By choosing initial and final values, $(\theta_0, \dot{\theta}_0)$, $(\theta_\mathrm{f}, \dot{\theta}_\mathrm{f})$, and solving for the control input, F, contained in $\gamma(\theta)$, it is now possible to find the needed input to achieve a trajectory in the $(\theta, \dot{\theta})$-plane connecting the two chosen points, assuming such a trajectory exist.

The first step in accomplishing the task presented in *Introduction* chapter 1 is to raise the pendulum high enough that it would be able to pass through the obstacles. It is be possible to clear a straight path through the obstacles by raising the pendulum from the starting position of $\theta = \pi$ to a little less than $\theta = \frac{\pi}{2}$. Further, the velocity would ideally achieve zero angular velocity as it reaches its target angle. This idea is presented in Figure 5.1, without restricting the pendulum to a specific trajectory but rather showing the initial and final conditions.

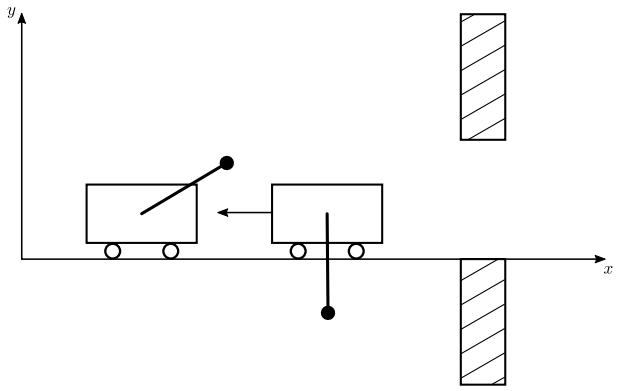

Figure 5.1: The first task is to find a trajectory which raises the pendulum to a position where it is clear of the obstacles in the horizontal direction. Further, to maintain clearance, the angular velocity should hit zero as the target angle is achieved.

Assuming that the pendulum was raised above $\frac{\pi}{2}$ while briefly achieving zero angular velocity, the next task would be to maintain zero angular velocity while moving the cart, passing the pendulum through the obstacles, see Figure 5.2.

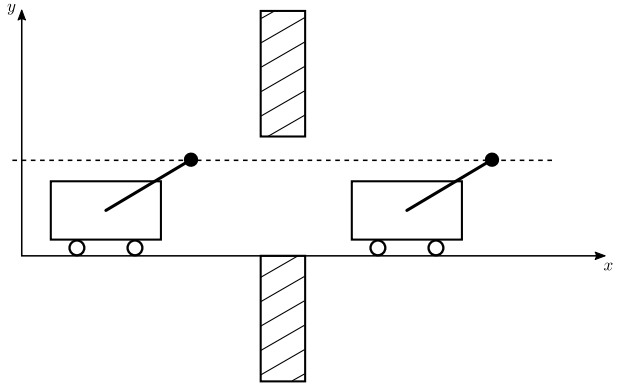

Figure 5.2: The second task is to find a trajectory which keeps the angle and angular velocity at zero as the pendulum is moved with the cart through the obstacles. This can be seen as a virtual constraint where the pendulum mass is constrained to the dotted line.

Ideally this trajectory is a straight horizontal line. This can be seen as a virtual constraint that forces the angle and the angular velocity to stay unchanged. The result will be significantly reduced dynamics, which can be used to directly achieve the desired trajectory.

Finally it is necessary to recover the system on the other side of the obstacles. It is found that this can be achieved, to some extend, by reversing the first trajectory.

6 | First Trajectory

Firstly the initial and final values of of θ and $\dot{\theta}$ are known. Further, the θ-dynamics are known, also for non-zero forces. In the state space and general equations, Equation 5.6 and Equation 5.2, the input force is contained by the γ-function.
The problem to be solved is the integral in Equation 5.16, which perserves its zero value along the trajectory from initial to final value assuming the solution exist. It is noted that $\alpha(\theta) > 0$ for any real value of θ in this system as is required. The initial values are $(\theta_0, \dot{\theta}_0) = (\pi, 0)$ and the final values are chosen to be $(\theta_f, \dot{\theta}_f) = (\frac{7\pi}{4}), 0$, which should should achieve a reasonable starting point for the next trajectory. It turns out, that in this case the problem can be solved analytically. To break up the problem, Equation 5.16 is rewritten as,

$$I(\theta, \dot{\theta}, \theta_0, \dot{\theta}_0) = \dot{\theta}^2 - \psi(\theta_0, \theta) \left(\dot{\theta}_0^2 - \int_{\theta_0}^{\theta} \psi(s, \theta_0) \frac{2\gamma(s)}{\alpha(s)} ds \right) \quad , \tag{6.1}$$

where,

$$\psi(\theta_1, \theta_2) = \exp \left[-2 \int_{\theta_1}^{\theta_2} \frac{\beta(\tau)}{\alpha(\tau)} d\tau \right] \quad .$$

For this trajectory, both the the initial and final angular velocity, $\dot{\theta}_0$ and $\dot{\theta}_f$, are zero, so $\dot{\theta}_0^2 = 0$ and $\dot{\theta}^2 = 0$, in Equation 6.1.
For the pendulum,

$$\psi(\theta_1, \theta_2) = \exp \left[-2 \int_{\theta_1}^{\theta_2} \frac{\frac{m^2 l^2}{M+m} \cos\tau \sin\tau}{ml^2 - \frac{m^2 l^2}{M+m} \cos^2\tau} d\tau \right] \quad .$$

Applying u-substitution to solve this exponential integral and inserting the general limits results in,

$$\psi(\theta_1, \theta_2) = \frac{ml^2 - \frac{m^2 l^2}{M+m} \cos^2\theta_1}{ml^2 - \frac{m^2 l^2}{M+m} \cos^2\theta_2} \quad . \tag{6.2}$$

For each set of limits,

$$\psi(\theta_0, \theta) = \frac{ml^2 - \frac{m^2 l^2}{M+m} \cos^2\theta_0}{ml^2 - \frac{m^2 l^2}{M+m} \cos^2\theta} \Bigg|_{\theta_0=\pi} = \frac{ml^2 - \frac{m^2 l^2}{M+m}}{ml^2 - \frac{m^2 l^2}{M+m} \cos^2\theta} \quad , \tag{6.3}$$

and

$$\psi(s, \theta_0) = \frac{ml^2 - \frac{m^2 l^2}{M+m} \cos^2 s}{ml^2 - \frac{m^2 l^2}{M+m} \cos^2\theta_0} \Bigg|_{\theta_0=\pi} = \frac{ml^2 - \frac{m^2 l^2}{M+m} \cos^2 s}{ml^2 - \frac{m^2 l^2}{M+m}} \quad . \tag{6.4}$$

Inserting these results, Equation 6.3 and Equation 6.4, along with the expressions for $\alpha(s)$ and $\gamma(s)$ into Equation 6.1 yields,

$$I(\theta,\dot{\theta},\theta_0,\dot{\theta}_0) = \frac{ml^2 - \frac{m^2l^2}{M+m}}{ml^2 - \frac{m^2l^2}{M+m}\cos^2\theta}\left(-\int_{\theta_0}^{\theta}\frac{ml^2 - \frac{m^2l^2}{M+m}\cos^2 s}{ml^2 - \frac{m^2l^2}{M+m}}\cdot\frac{2(-mgl\sin s - \frac{ml}{M+m}\cos sF)}{ml^2 - \frac{m^2l^2}{M+m}\cos^2 s}ds\right)$$

$$I(\theta,\dot{\theta},\theta_0,\dot{\theta}_0) = \frac{ml^2 - \frac{m^2l^2}{M+m}}{ml^2 - \frac{m^2l^2}{M+m}\cos^2\theta}\left(-2\int_{\theta_0}^{\theta}\frac{-mgl\sin s - \frac{ml}{M+m}\cos sF}{ml^2 - \frac{m^2l^2}{M+m}}ds\right) \tag{6.5}$$

$$I(\theta,\dot{\theta},\theta_0,\dot{\theta}_0) = \frac{ml^2 - \frac{m^2l^2}{M+m}}{ml^2 - \frac{m^2l^2}{M+m}\cos^2\theta}\left(-4\left[\frac{Mg+mg-F\tan\frac{s}{2}}{Ml(\tan^2\frac{s}{2}+1)}\right]_{\theta_0}^{\theta}\right) \quad . \tag{6.6}$$

Inserting initial and final value of θ and solving for F, the force which creates the desired trajectory is obtained. Also note that for this trajectory the applied force is constant and negative, pulling the cart to the left.

7 | Second and Third Trajectory

The second trajectory to complete the task seen in Figure 5.2 is different than the first, in that it does not require movement in the $(\theta, \dot{\theta})$-plane, in fact, rather the contrary. It does however require the cart to move forward in order to pass the obstacles and hold up the pendulum.
As before, the initial values are known and a final position of the cart can be chosen, which will be the condition for switching to the final task.
Substituting the initial and final values, $\theta = \theta_\mathrm{f}$, $\dot{\theta} = 0$ and $\ddot{\theta} = 0$, into Equation 5.1, reduces the dynamics to,

$$\begin{cases} -ml\cos\theta_\mathrm{f}\ddot{x} - mgl\sin\theta_\mathrm{f} = 0 \\ (M+m)\ddot{x} = F \quad . \end{cases} \qquad [\cdot] \quad (7.1)$$

In Equation 7.1 the force, F, is directly provided as a function of the acceleration of the cart. Feeding back $\ddot{x}$ in this manner will attempt to keep the angle of the pendulum steady while moving forward through the obstacles.

For the third and final trajectory, the idea is to stop the system. This is achieved using Equation 6.6, where $(\theta_0, \dot{\theta}_0) = (\frac{7\pi}{8}, 0)$ and the final values, $(\theta, \dot{\theta} = (\pi, 0)$. While this does bring the pendulum to rest, the cart still has momentum and will drag the pendulum out of equilibrium after which the system is caught in a stable orbit since there is no friction to dampen the oscillations. This issue was not solved during this project.

Bibliography

[1] *Maxon Motor*. Aug. 15, 2018. URL: https://www.maxonmotor.com/maxon/view/product/motor/dcmotor/re/re50/370356.

[2] Avago Technologies. *HEDM-55xx/560x & HEDS-55xx/56xx*. Aug. 15, 2018. URL: https://www.infineon.com/dgdl/Infineon-Encoder_HEDS-5540-A14-AP-v01_00-EN.pdf?fileId=5546d46147a9c2e40147d3d593970357.

[3] *Maxon Controller*. Aug. 15, 2018. URL: https://www.maxonmotor.com/maxon/view/product/control/Servoverstaerker-4-Q-DC/201583.

[4] *K66 Sub-Family Reference Manual*. Aug. 15, 2018. URL: https://cdn.sparkfun.com/datasheets/Dev/Arduino/Boards/K66P144M180SF5RMV2.pdf.

[5] *sparkfun Teensy 3.6*. Aug. 15, 2018. URL: https://www.sparkfun.com/products/14057.

[6] *HCTL-2021 PLC Avago Datasheet*. Aug. 15, 2018. URL: https://datasheet.octopart.com/HCTL-2021-PLC-Avago-datasheet-7580518.pdf.

[7] Jonas Ørndrup Jesper H. Hørgensen. *Non-linear Control and Machine Learning on an Inverted Pendulum on a Cart. Master Thesis*. 2018.

[8] Mark W. Spong, Seth Hutchinson, and M. Vidyasagar. *Robot Dynamics and Control*. 2nd ed. Wiley, 2005.

[9] Lorenzo Sciavicco and Bruno Siciliano. *Modelling and Control of Robot Manipulators*. 2nd ed. Lorenzo Sciavicco and Bruno Siciliano. London: Springer, 2012.

[10] Carlos Canudas-de-Wit Anthon Shiriaev John W. Perram. "Constructive Tool for Orbital Stabilization of Underactuated Nonlinear Systems: Virtual Constraints Approach". In: *IEEE Transactions on Automation and Control VOL. 50, NO 8. August* (2005).